Large Eddy Simulation (LES) for IC Engine Flows

Tang-Wei Kuo, Xiaofeng Yang, Venkatesh Gopalakrishnan, Zhaohui Chen

© Photos: DOI: 10.2516/ogst/2013139, IFPEN, X

Dossier

This paper is a part of the hereunder thematic dossier published in OGST Journal, Vol. 69, No. 1, pp. 3-188 and available online here

Cet article fait partie du dossier thématique ci-dessous publié dans la revue OGST, Vol. 69, n°1, pp. 3-188 et téléchargeable ici

DOSSIER Edited by/Sous la direction de : **C. Angelberger**

IFP Energies nouvelles International Conference / Les Rencontres Scientifiques d'IFP Energies nouvelles

LES4ICE 2012 - Large Eddy Simulation for Internal Combustion Engine Flows

LES4ICE 2012 - La simulation aux grandes échelles pour les écoulements dans les moteurs à combustion interne

Oil & Gas Science and Technology – Rev. IFP Energies nouvelles, Vol. 69 (2014), No. 1, pp. 3-188

Oil & Gas Science and Technology – Rev. IFP Energies nouvelles, Vol. 69 (2014), No. 1, pp. 61-81

DOI: 10.2516/ogst/2013127

IFP Energies nouvelles International Conference
Rencontres Scientifiques d'IFP Energies nouvelles

LES4ICE 2012 - Large Eddy Simulation for Internal Combustion Engine Flows
LES4ICE 2012 - La simulation aux grandes échelles pour les écoulements dans les moteurs à combustion interne

Large Eddy Simulation (LES) for IC Engine Flows

Tang-Wei Kuo*, Xiaofeng Yang, Venkatesh Gopalakrishnan and Zhaohui Chen

General Motors Global Research & Development, Warren, MI - USA
e-mail: tang-wei.kuo@gm.com - xiaofeng.yang@gm.com - venkatesh.gopalakrishnan@gm.com - zhaohui.chen@gm.com

* Corresponding author

Résumé — **Simulations des grandes échelles et écoulements dans les moteurs à combustion interne** — Des calculs numériques ont été effectués en utilisant un modèle de simulation des grandes échelles (*Large Eddy Simulation*, LES) à l'échelle de l'ingénierie fournie par le code commercial CFD CONVERGE. Le cadre analytique et l'installation expérimentale consistent en un moteur monocylindre en marche doté d'une chambre de combustion transparente (*Transparent Combustion Chamber*, TCC). Une procédure rigoureuse de travail pour la comparaison et l'analyse des résultats des simulations et des expériences de vélocimétrie par imagerie de particules (*Particle Image Velocimetry*, PIV) à haute vitesse est présentée dans ce document. Les aspects suivants de la LES sont analysés en utilisant cette procédure :
– nombre de cycles requis pour obtenir une convergence à la précision voulue ;
– effet de la taille de maille, du pas de temps, des modèles de turbulence aux échelles inférieures à la maille (*sub-grid-scale*, SGS) et du traitement des conditions aux limites ;
– application d'une technique de décomposition orthogonale aux valeurs propres (*Proper Orthogonal Decomposition*, POD).

Abstract — ***Large Eddy Simulation (LES) for IC Engine Flows*** — *Numerical computations are carried out using an engineering-level Large Eddy Simulation (LES) model that is provided by a commercial CFD code CONVERGE. The analytical framework and experimental setup consist of a single cylinder engine with Transparent Combustion Chamber (TCC) under motored conditions. A rigorous working procedure for comparing and analyzing the results from simulation and high speed Particle Image Velocimetry (PIV) experiments is documented in this work. The following aspects of LES are analyzed using this procedure:*
– *number of cycles required for convergence with adequate accuracy;*
– *effect of mesh size, time step, sub-grid-scale (SGS) turbulence models and boundary condition treatments;*
– *application of the proper orthogonal decomposition (POD) technique.*

INTRODUCTION

New automotive engine technologies promise to achieve improved fuel economy with reduced emissions. However, these technologies are more sensitive to stochastic processes and can suffer from increased cyclic variability. Large Eddy Simulation (LES) is an important computational tool for understanding the critical processes that impact cyclic variability, and eventually can be used to minimize or eliminate their occurrence.

A concerted experimental and numerical effort is undertaken to understand and describe the nature of stochastic flows in internal combustion engines [1]. The overall goal is to develop physics-based computational tools for a more effective design of internal combustion engines of the future.

A working group was formed to develop the tools and processes for using LES effectively and accurately in IC engine analysis. The group incorporates members with expertise in LES modeling and engine experiments. The members work together closely to coordinate all aspects of the planning, configuration, modeling, data acquisition, analysis and evaluation of findings. The LES modeling group uses multiple simulation tools including commercial software, open-source codes and very high-resolution US National Laboratory flow solvers. The experimental work uses high accuracy, detailed planar and 3D optical diagnostics for in-cylinder flow and combustion analysis.

The engine configuration used in current work consists of a simple cylindrical combustion chamber for non-reacting flow and homogeneous-charge combustion analysis. The cylindrical combustion chamber has a simple geometry with well-controlled boundary conditions. Hence, it is relatively easy to simulate and also conduct experiments with high accuracy measurements.

This paper summarizes *GM* R&D's efforts on numerical simulation of non-reacting flow using an engineering-level LES approach. The work addresses the following questions:

– What are proper working procedures for quantitative comparisons between PIV-measured and LES-calculated results?
– What is an adequately accurate LES prediction?
– What is the best use of LES-calculated results?

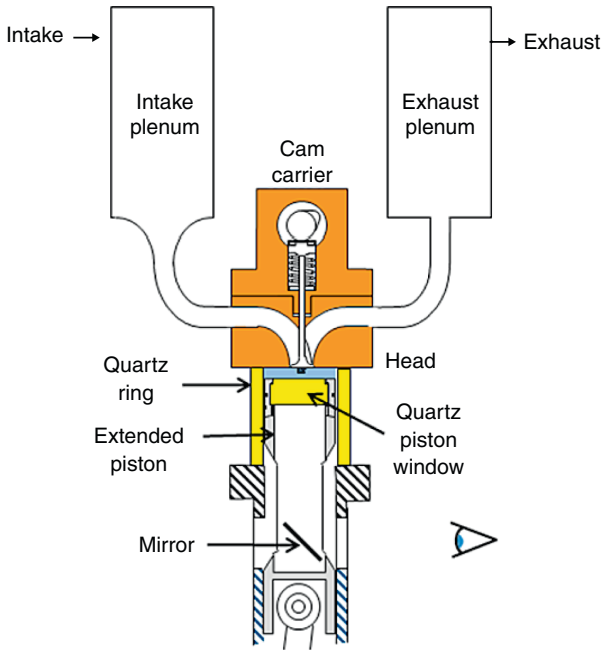

Figure 1
The Transparent Combustion Chamber (TCC) Engine.

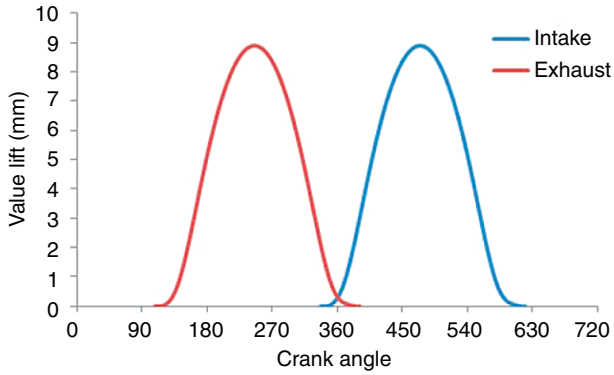

Figure 2
Intake and exhaust valve lift.

1 THE EXPERIMENT

1.1 Experimental Setup

An optical engine test setup was developed for the specific purpose of supporting the development and validation of a range of LES approaches. The test setup features a single cylinder optical engine connected to intake and exhaust plenums *via* intake and exhaust runners, respectively. Figure 1 shows the engine features: a two-valve head and simple intake and exhaust port geometries with a pancake-shape combustion chamber. Figure 2 shows the intake and exhaust valve

lift profiles. Table 1 lists the details of engine specifications and Table 2 lists the intake and exhaust geometries.

TABLE 1
TCC engine specifications

Bore	92.00	mm
Stroke	86.00	mm
Connecting rod length	234.95	mm
Wrist pin to crank offset	0.00	mm
TDC clearance height	9.50	mm
Top land crevice volume	0.42	L
Geometric compression ratio	10.00	
Engine speed	800	rpm
Average intake plenum temperature	45.0	°C
Average intake plenum pressure	95.0	kPa
Average exhaust plenum pressure	101.5	kPa

1.2 GT-Power Model

The wave dynamics of complete engine experimental setup is simulated with a detailed 1-D flow model, GT-Power. This model includes the entire intake and exhaust system in the test cell from the critical orifice flow metering setup to the exhaust throttle valve (*Fig. 3*). The 1-D model is validated with experimental measurements and used to provide the boundary conditions for LES calculations. In particular, Figure 4 shows quantitative comparisons between measured and GT-Power-calculated pressure results. The agreement between measured and calculated pressures is quite good at selected monitoring locations.

2 LARGE EDDY SIMULATION MODEL DESCRIPTION

A LES approach at an engineering-level is evaluated with the CONVERGE code [2] at *GM* R&D. The code is capable of simulating three-dimensional, incompressible/compressible, unsteady, turbulent, chemically reacting fluid flows in complex geometries. The solver can handle arbitrary number of species and chemical reactions and unsteady liquid sprays. Currently, two LES models are implemented in the code:

– Smagorinsky viscosity model [3, 4],
– one-equation eddy viscosity model [5-8], which adds a transport equation for sub-grid kinetic energy which is then employed to model the turbulent viscosity.

TABLE 2
TCC engine intake and exhaust geometries

Component	Diameter (mm)	Length (mm)	Radius of bend (mm)	Angle of bend (°)
Intake plenum inlet	25.4	1500.0	0.0	0.0
Intake plenum	177.9	609.6	0.0	0.0
Intake flange	25.4	25.4	38.1	0.0
Intake runner	25.4	119.7	76.2	90.0
Intake runner to port	25.4	106.5	0.0	0.0
Intake port	25.4	94.24	59.9	90.0
Exhaust port	25.4	94.24	59.9	90.0
Exhaust port to runner	25.4	68.2	0.0	0.0
Exhaust runner	25.4	119.7	76.2	90.0
Exhaust flange	25.4	46.1	0.0	0.0
Exhaust plenum	177.9	590.5	0.0	0.0
Exhaust plenum outlet	25.4	140.0	0.0	0.0

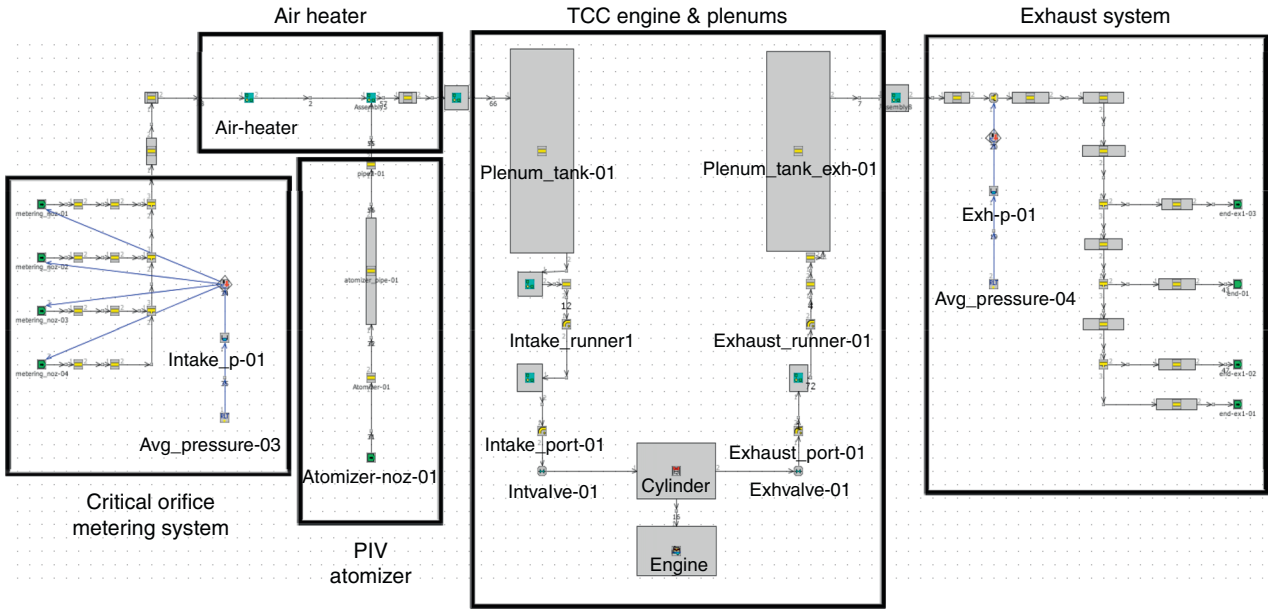

Figure 3

1-D GT-Power model of TCC engine.

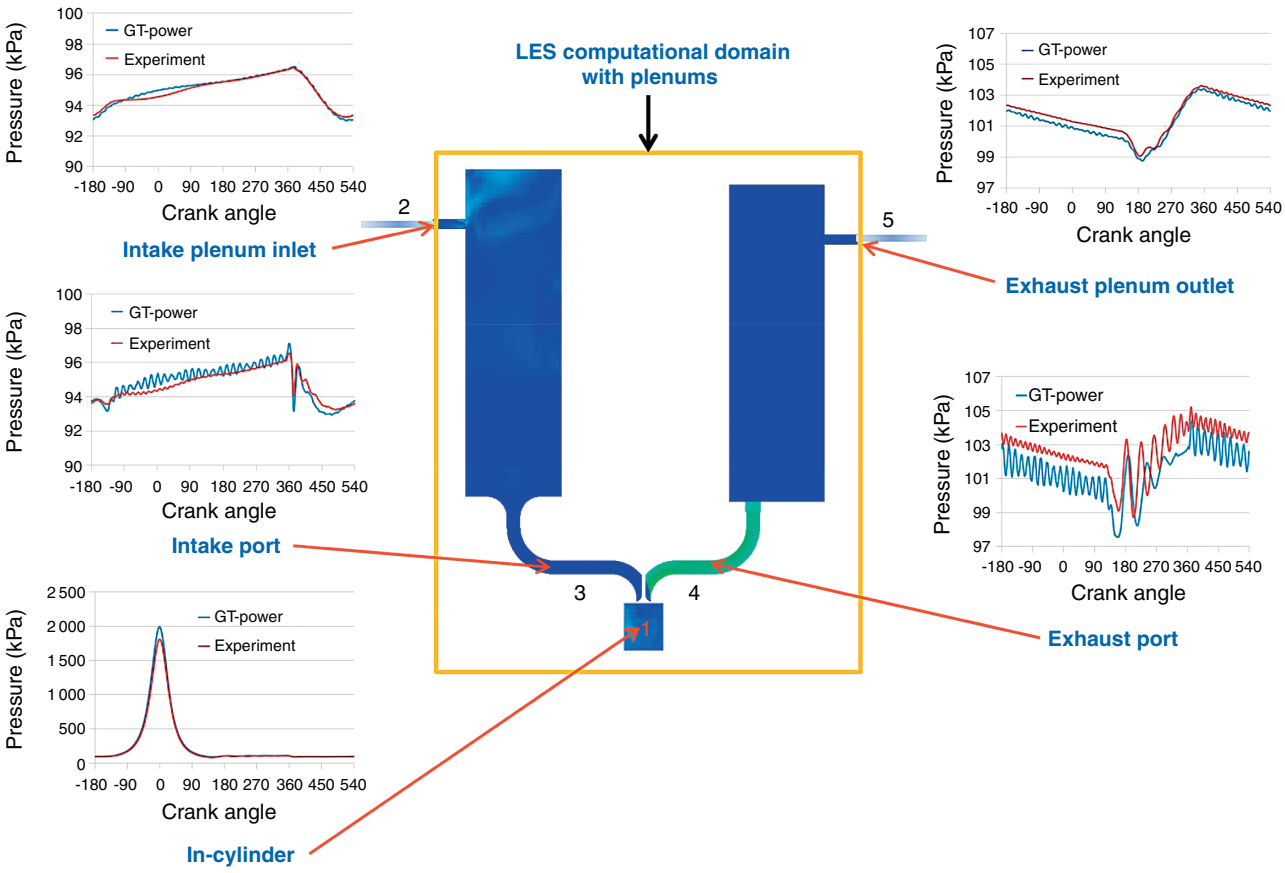

Figure 4

LES computational domain, measurement locations, measured and calculated pressure traces.

2.1 Smagorinsky Viscosity Model

The Smagorinsky model is a zero equation LES model which relates the turbulent viscosity to magnitude of the strain rate tensor and cell size. The turbulent viscosity is given by:

$$v_t = C_s^2 \Delta^2 \sqrt{2 S_{ij} S_{ij}} \tag{1}$$

Here, Δ is filter size which is related to the cell volume by the following expression:

$$\Delta = \sqrt[3]{Vol} \tag{2}$$

The Smagorinsky model can be 'tuned' by adjusting the constant C_s in the expression for turbulent viscosity.

2.2 One-Equation Eddy Viscosity Model

The one-equation viscosity model adds a transport equation for the sub-grid kinetic energy. The sub-grid kinetic energy is then used in modeling the turbulent viscosity. The sub-grid kinetic energy equation is given by:

$$\frac{\partial k}{\partial t} + \bar{u_i} \frac{\partial k}{\partial x_i} = -\tau_{ij} \frac{\partial \bar{u_i}}{\partial x_j} - \epsilon + \frac{\partial}{\partial x_i} \left(\frac{v_t}{\sigma_k} \frac{\partial k}{\partial x_i} \right) \tag{3}$$

Here, the sub-grid kinetic energy is given by:

$$k = \frac{1}{2} \left(\overline{u_i u_j} - \overline{u_i} \overline{u_j} \right) \tag{4}$$

The turbulent viscosity for the one-equation model is given as:

$$v_t = C_k k^{1/2} \Delta \tag{5}$$

The turbulent viscosity can be 'tuned' by adjusting the constant C_k in the above expression. The sub-grid dissipation is given as:

$$\epsilon = C_\varepsilon k^{3/2} / \Delta \tag{6}$$

The sub-grid dissipation can also be 'tuned' by adjusting the constant C_ε in the above expression.

Table 3 summarizes the LES model constants and their recommended values. They were kept unchanged for all the results presented in this paper. Further, when running the LES model with CONVERGE, it is recommended that the Werner and Wengle wall model [9] be enabled.

Orthogonal cubic meshes are automatically created at run time to avoid any variation in cell shape or size. Adaptive Mesh Refinement (AMR) can also be used to increase the effective grid resolution but is not enabled in the present study. The sub-grid stress tensor that is being modeled by LES can be shown to be 2nd order in accuracy.

TABLE 3
LES model constants

LES model constants	Recommended value
C_S	0.1 to 1.0 (0.05 used in this study)
C_k	0.05
C_ε	1.0

A special feature of the code called 'embed-sphere' was employed in all the LES calculations carried out at *GM* R&D. This is mainly to minimize the effect of mesh topology on the computed results and to enable better quantitative comparisons between various applications. An example is shown in Figure 5 where the finest mesh (1 mm) is placed in cylinder and port regions while the coarsest mesh (8 mm) is placed inside the intake and exhaust plenums.

3 PROPER ORTHOGONAL DECOMPOSITION (POD) ANALYSIS METHODOLOGY

The Proper Orthogonal Decomposition (POD) is used to analyze and compare the complex in-cylinder flows from both the LES and the PIV measurements [10]. The fundamental idea behind proper orthogonal decomposition is to decompose a time-dependent velocity field, $\boldsymbol{u}(\boldsymbol{x}, t)$, into a linear combination of $\boldsymbol{M}$ spatial basis functions (the POD modes, denoted $\psi^{(k)}(\boldsymbol{x})$) and the corresponding time-dependent coefficients (denoted $a^{(k)}(t)$):

$$\boldsymbol{u}(\boldsymbol{x}, t) = \sum_{k=1}^{M} \left(a^{(k)}(t) \psi^{(k)}(\boldsymbol{x}) \right) \tag{7}$$

In practice, this is done using samples of the velocity field obtained at discrete spatial locations and at discrete instants in time, obtained from experiment or from simulation. In POD, the basis functions are not specified *a priori*; rather, they are computed from the velocity field itself. Key properties of POD modes are: the original velocity field can be expressed as a linear combination of POD modes; the POD modes are mutually orthogonal and of unity magnitude; and the POD modes are optimal in the sense that a higher fraction of the original flow's kinetic energy can be captured using fewer POD modes compared to any other orthogonal basis. Details of the theory and method of calculation can be found in [11].

In most applications to turbulent flows, the POD modes have been found using the "method of snapshots"

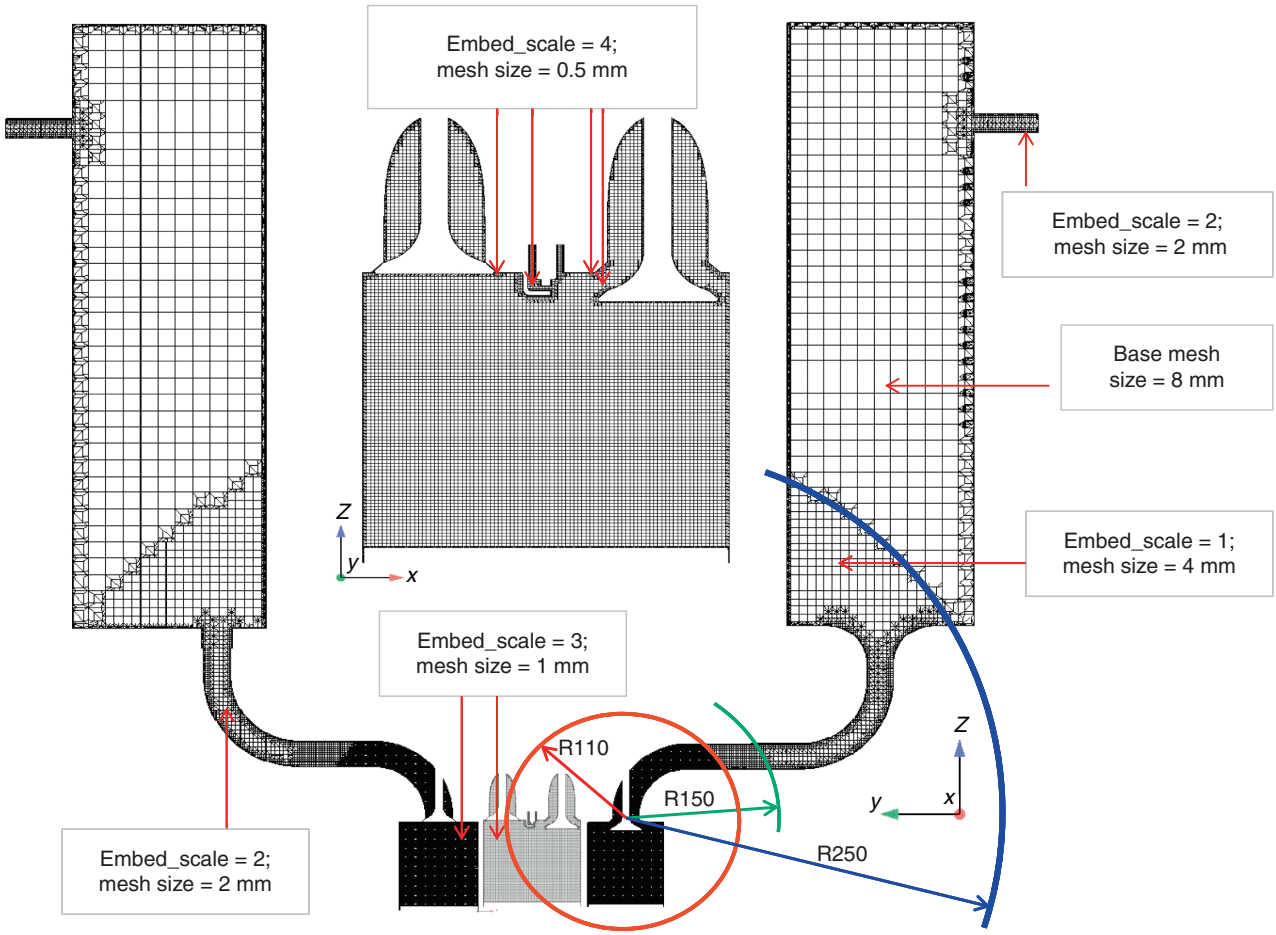

Figure 5

Mesh arrangement for the fine mesh with in-cylinder mesh size of 1 mm.

introduced by Sirovich [12]. The method of snapshots is equivalent to the more formal direct method for computing the POD [11, 13] and is computationally less intensive, especially in cases where the number of spatial locations at which the velocity field is sampled is greater than the number of instants in time at which it is sampled. The method of snapshots is the approach that has been adopted here. The algorithm for extracting the POD modes that are required to deal with flows in piston engines, and other aspects of POD-based analysis that are relevant to the engine application can be found in [10].

It is useful to have a quantitative measure of the degree to which two velocity fields are similar or dissimilar. Such a criterion can be used to compare a velocity field obtained from simulation with a velocity field obtained from experiment, to compare a POD mode with a velocity field obtained from simulation or from experiment, or to compare two POD modes that were obtained using different methods of analysis (*e.g.*, phase-dependent analysis *versus* phase-invariant analysis). One such criterion is the "relevance index" $f_{u,v}$ that is obtained by projecting one velocity field $\boldsymbol{u}$ onto another velocity field $\boldsymbol{v}$:

$$f_{u,v} = \frac{(\boldsymbol{u}, \boldsymbol{v})}{||\boldsymbol{u}||\ ||\boldsymbol{v}||} \tag{8}$$

In the equation above, the numerator is the inner product of two velocity fields over the whole domain. The value of the relevance index $f_{u,v}$ varies from -1 to $+1$; a value of $+1$ means that the two velocity fields are identical, while a value of -1 means that they are exactly opposite to each other. The velocity fields, $\boldsymbol{u}$ and $\boldsymbol{v}$ are orthonormal if $f_{u,v}$ is equal to 0. The relevance index of Equation (8) has been adopted as a quantitative basis for comparing velocity fields in Section 4.

4 RESULTS AND DISCUSSION

Quantitative comparison of LES results with high-speed PIV measurements is essential to evaluate the accuracy of the simulation. The primary evaluation criteria are:

– mean and RMS velocities: the statistical quantities of ensemble-mean and RMS velocity values are compared between high-speed PIV measurements and LES computations at two different crank angle positions; one during intake at 100 degrees After Top Dead Center Exhaust (ATDCE) and another near top dead center compression at 300 degrees ATDCE;
– Proper Orthogonal Decomposition (POD) energy fractions and modes: quantitative comparison of the energy fractions is carried out at the above mentioned crank angle positions. Development of tools for 2D and 3D phase-dependent and phase-invariant POD analysis of full motored 720-degree engine cycles or sub-cycles along with combined analysis of samples from both the LES and PIV measurements to form a common basis were investigated by the LES working group. In this paper, only 2D phase-dependent POD results are presented and discussed. More results on POD analysis from the working group are presented in two additional papers at the LES4ICE 2012 Conference [14, 15].

The results from the baseline (Case 1) calculations are presented and discussed first. Sensitivity analysis of results that show the effects of numerical parameters, Sub-Grid-Scale (SGS) viscosity models and boundary conditions then follow. All the cases are listed in Table 4 and are grouped as shown below:

– in-cylinder mesh size of 1 mm (Case 1), 0.75 mm (Case 2) and 2 mm (Case 3), respectively,
– adaptive time step (Case 1), as determined by the CFD code during execution, *versus* minimum fixed time step (Case 4),
– zero-equation (Smagorinsky, Case 5) and one-equation (Case 1) SGS viscosity models,
– with and without GT-Power calculated boundary condition specifications (Cases 1, 6-8).

The POD energy fractions in the first mode over the POD analysis window (to be discussed in *Fig. 7*

TABLE 4
Calculation matrix

Case #	Boundary and inlet conditions		Mesh Size	Time Step	LES Model	10-Cycle mode 1 energy fraction @ 100 degree ATDCE	10-Cycle mode 1 energy fraction @ 300 degree ATDCE
PIV						0.645 (56 cycles) 0.692 (10 cycles)	0.796 (56 cycles) 0.825 (10 cycles)
1(Baseline)	Time varying Total pressure	Time varying Temperature	1 mm	> 4.8e-6 s	1-Eqn viscosity	0.569 (56 cycles) 0.607 (10 cycles)	0.814 (56 cycles) 0.837 (10 cycles)
2			0.75 mm	> 4.8e-6 s	1-Eqn viscosity	0.577 (10 cycles)	0.760 (10 cycles)
3			2 mm	> 4.8e-6 s	1-Eqn viscosity	0.728 (10 cycles)	0.857 (10 cycles)
4			1 mm	2e-6 s	1-Eqn viscosity	0.616 (10 cycles)	0.850 (10 cycles)
5			1 mm	> 4.8e-6 s	0-Eqn viscosity	0.587 (10 cycles)	0.819 (10 cycles)
6	Fixed total pressure (95 kPa)	Fixed temperature (45°C)	1 mm	> 4.8e-6 s	1-Eqn viscosity	0.542 (10 cycles)	0.842 (10 cycles)
7	1-D predicted mass flow rate	1-D predicted temperature	1 mm	> 4.8e-6 s	1-Eqn viscosity	0.597 (10 cycles)	0.820 (10 cycles)
8	1-D predicted static pressure	1-D predicted temperature	1 mm	> 4.8e-6 s	1-Eqn viscosity	0.636 (10 cycles)	0.871 (10 cycles)

in *Sect. 5.2*) for all the cases are also listed in Table 4 for later discussion.

5 BASELINE (CASE 1)

5.1 Convergence, Sampling and Number of Engine Cycles

While the experimental cycles are completed in real time, the computational cycles using LES take a relatively long time to complete. Hence, a prudent approach to minimize the number of computational cycles to reach steady state engine operation is essential. Experimental data is acquired after the engine reaches a steady state operation in terms of speed, peak cylinder average pressure and intake pressure fluctuations. A 1-D model that was discussed earlier is calibrated and employed to capture the behavior of steady state experimental engine.

Figure 6 shows the computed peak cylinder average pressure and in-cylinder trapped mass from cycle-to-cycle using LES. It can be seen that $\pm 0.25\%$ fluctuation in peak cylinder average pressure is achieved in 10-cycles while $\pm 0.05\%$ fluctuation in in-cylinder trapped mass is achieved within first 3-cycles. Hence, 10-cycles are sufficient for cycle-to-cycle convergence of peak cylinder average pressure and trapped cylinder mass. It is to be noted that the LES computation employs converged initial and boundary conditions from the 1-D GT-Power model that is calibrated to the experimental setup. In reality, because of the size of the intake and exhaust surge tanks ($\sim$50 $\times$ displacement of engine cylinder), it will take close to 50 cycles to reach steady state.

Also, the peak cylinder average pressure fluctuation of $\pm 0.25\%$ is 5 times higher than that of the trapped mass ($\pm 0.05\%$) because the mean in-cylinder gas temperature also fluctuates such that the trapped mass fluctuations are much lower. Further, the experimental fluctuations are higher than predicted. We believe this is caused primarily by variations in mean gas temperature from cycle-to-cycle due to heat transfer and the simulations are not capturing this heat transfer accurately without using a conjugate heat transfer model. Further work is required in order to understand the sources of predicted peak cylinder average pressure variations.

5.2 Snapshot Crank Angle Degree and Field-of-View Window

In order to compare the spatially resolved flow field between LES and PIV measurements, snap shots of the flow field are taken at selected crank angle positions ATDCE. Figure 7 shows the POD analysis window chosen at two such crank angle positions, 100 and 300 degrees ATDCE. These two crank angle degrees are chosen in order to capture contrasting flow fields. At 100 degrees ATDCE, the air is inducted in the form of a powerful jet flowing through the intake passage by the downward motion of the piston. At 300 degrees ATDCE, the flow field is essentially free of any dominant bulk flow structures. The field of view for the POD analysis is shown as a red rectangular outline at these crank angles. This is chosen in order to ensure good reliability of experimental data from PIV measurements. Hence, a one-to-one comparison of LES results can be made with experimental data within these windows at 100 and 300 degrees ATDCE.

Several PIV data sets of varying lengths were available from the University of Michigan with the same nominal engine operating condition and minimal fluctuations in both engine speed ($\pm$ 1 rpm) and intake pressure ($\pm$ 0.01 kPa). One such set with 56 consecutive cycles is chosen in this paper. This is mainly because of the availability of 56 consecutive LES cycles for comparison.

Figure 8 shows the mean and RMS of the velocity measured using PIV at 100 and 300 degree ATDCE over 56 consecutive cycles. All the measurements are made after the engine is warmed up and is at steady state operation. Figure 9 shows the mean and RMS of the velocity computed using LES at 100 and 300 degree ATDCE over 56 consecutive cycles. The first 10 LES cycles from the start of computation are ignored in this analysis as the peak cylinder average pressure and trapped cylinder mass has not reached the quasi-steady state values (*Fig. 6*).

Comparing the experimental (*Fig. 8*) and LES (*Fig. 9*) results, it can be seen that there is fair agreement in both mean and RMS values at both crank angles as the calculated relevance index between 56-cycle average LES and PIV data over the POD analysis window indicated in Table 5. The authors do not expect the conclusions to change when a different set of 56 consecutive measured cycles are used. This is currently being verified as part of continuing work in this area by the working group.

The high RMS contours shown in PIV measurement near the intake jet region at 100 degree ATDCE is under-predicted by LES. There is concern that this may be due to dynamic range limitations in the experimental PIV data, especially when the high-speed intake jet flow is included in the analysis. However, new and improved PIV data does not support this argument. As a matter of fact, Figure 10 shows that by adding the SGS turbulent fluctuation u' (*Fig. 10c*) to LES-calculated RMS values (*Fig. 10b*), the agreement between

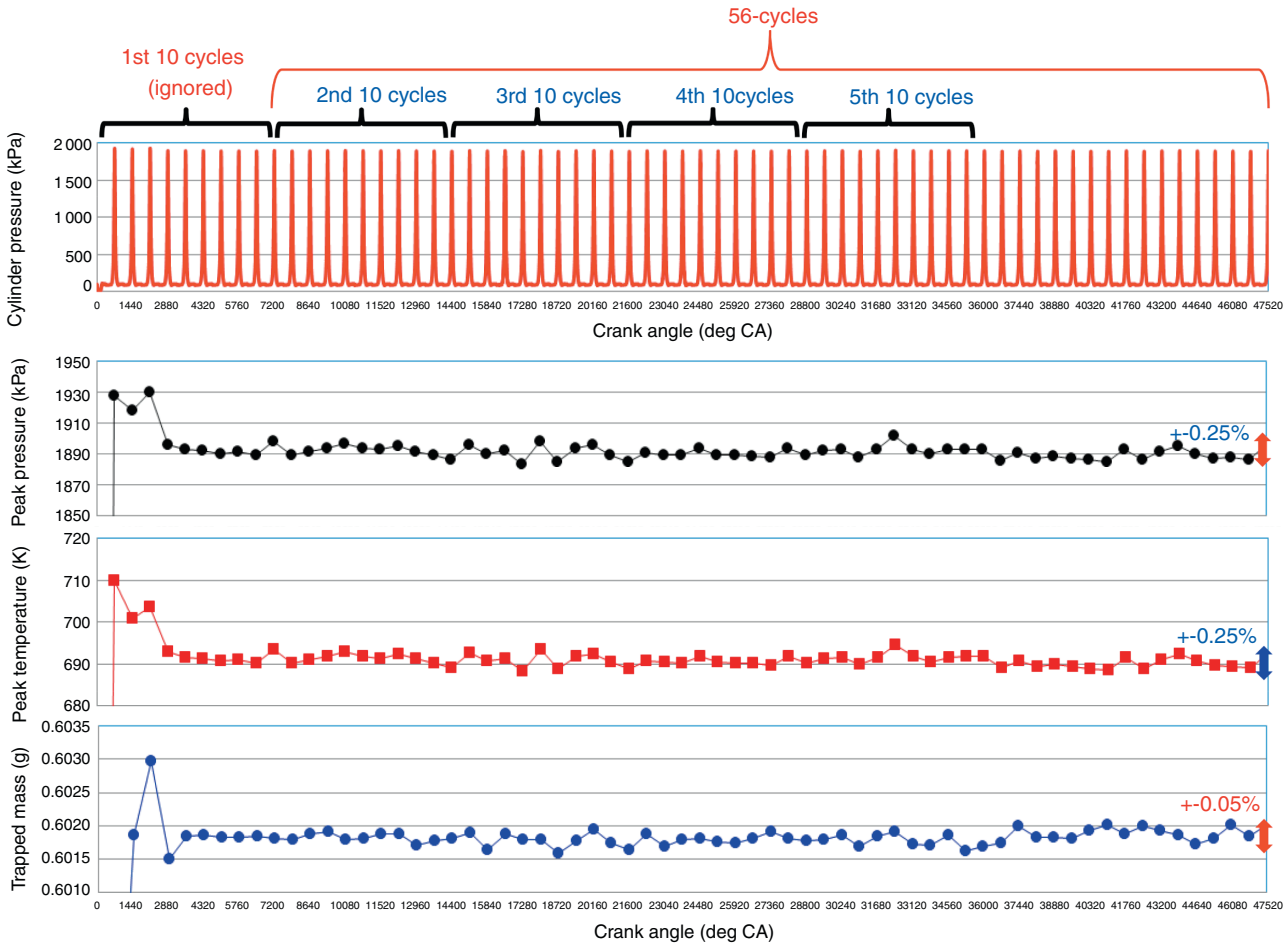

Figure 6

Calculated peak cylinder average pressure and trapped cylinder mass as a function of crank angle using LES.

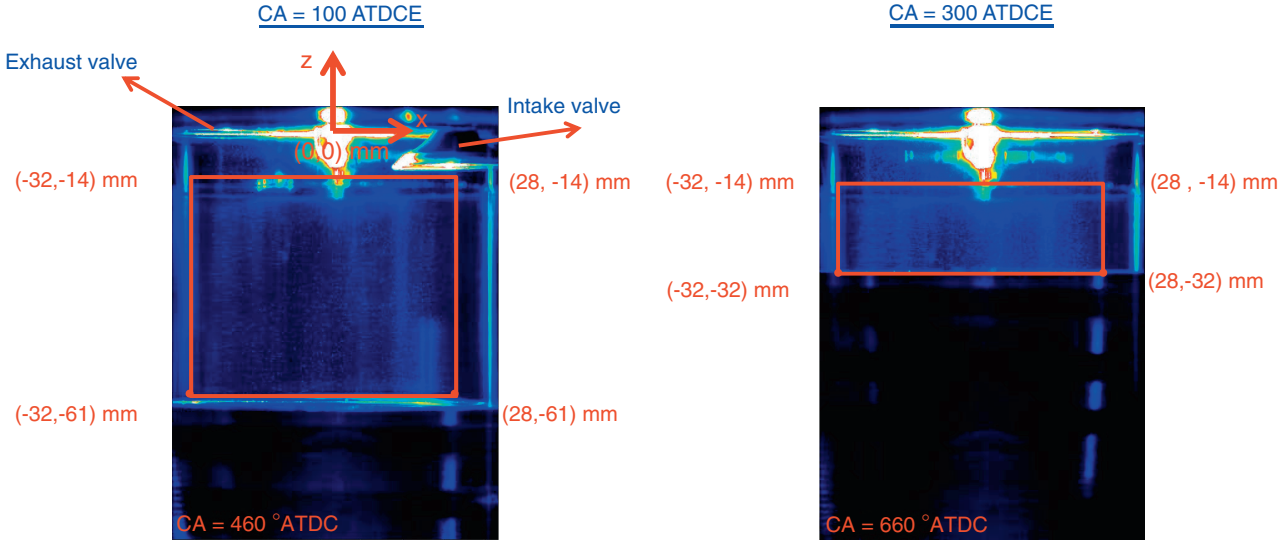

Figure 7

POD analysis windows at 100 and 300 degrees After Top Dead Center Exhaust (ATDCE).

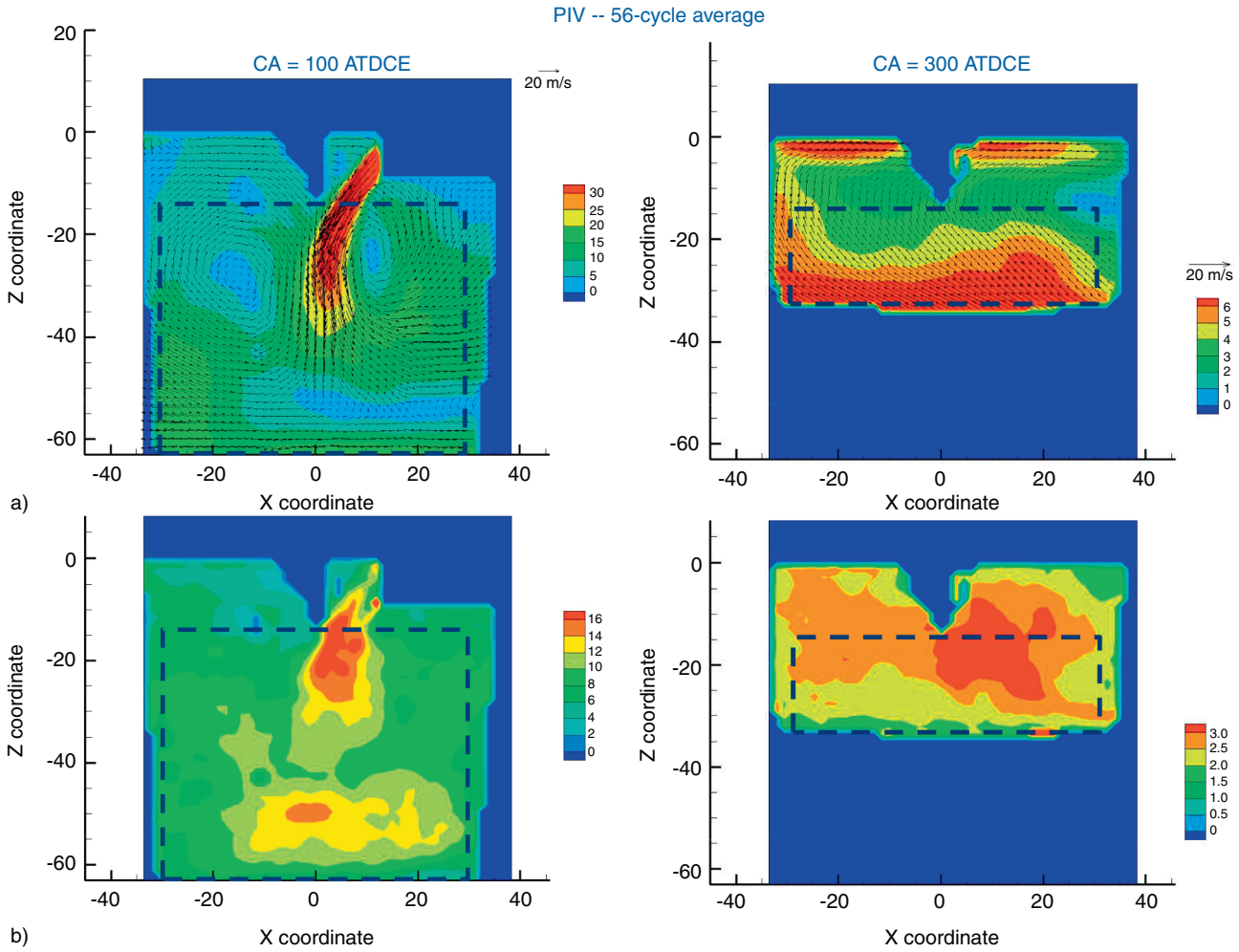

Figure 8

56-cycle average PIV results on a) mean and b) RMS velocities at 100 and 300 degree ATDCE.

PIV measurement (*Fig. 10a*) and LES prediction (*Fig. 10d*) is further improved. Similar observation can be made for RMS velocity at 300 degree ATDCE shown in Figure 11. The SGS turbulent fluctuation is calculated using $u' = \sqrt{2}\sqrt{2k/3}$ for two-dimensional turbulence.

In summary, LES predicted mean and RMS velocities agree well with the PIV measurements at both 100 and 300 degree ATDCE at the 2-D cutting plane. The results seem to suggest that 50-60 snapshots or cycles are sufficient from mean and RMS velocities standpoint.

Next step is to compare the energy fractions of the POD modes between LES and PIV measurements. Key properties of POD modes include:

– the original velocity field can be expressed as a linear combination of POD modes;
– the POD modes are computed from the velocity field itself rather than specified *a priori*;
– the POD modes are mutually orthogonal and of unity magnitude;
– the POD modes are optimal in the sense that a higher fraction of the original flow's kinetic energy can be captured using fewer POD modes compared to any other orthogonal basis;
– the POD modes should not be interpreted as (or POD modes has no direct linkage) to velocity structures.

Detailed analysis and discussion of POD modes can be found in [8, 12].

Table 4 shows that the energy fraction in the first mode over the POD analysis window is also dependent on the number of cycles. In general, the first mode energy fraction decreases with increasing

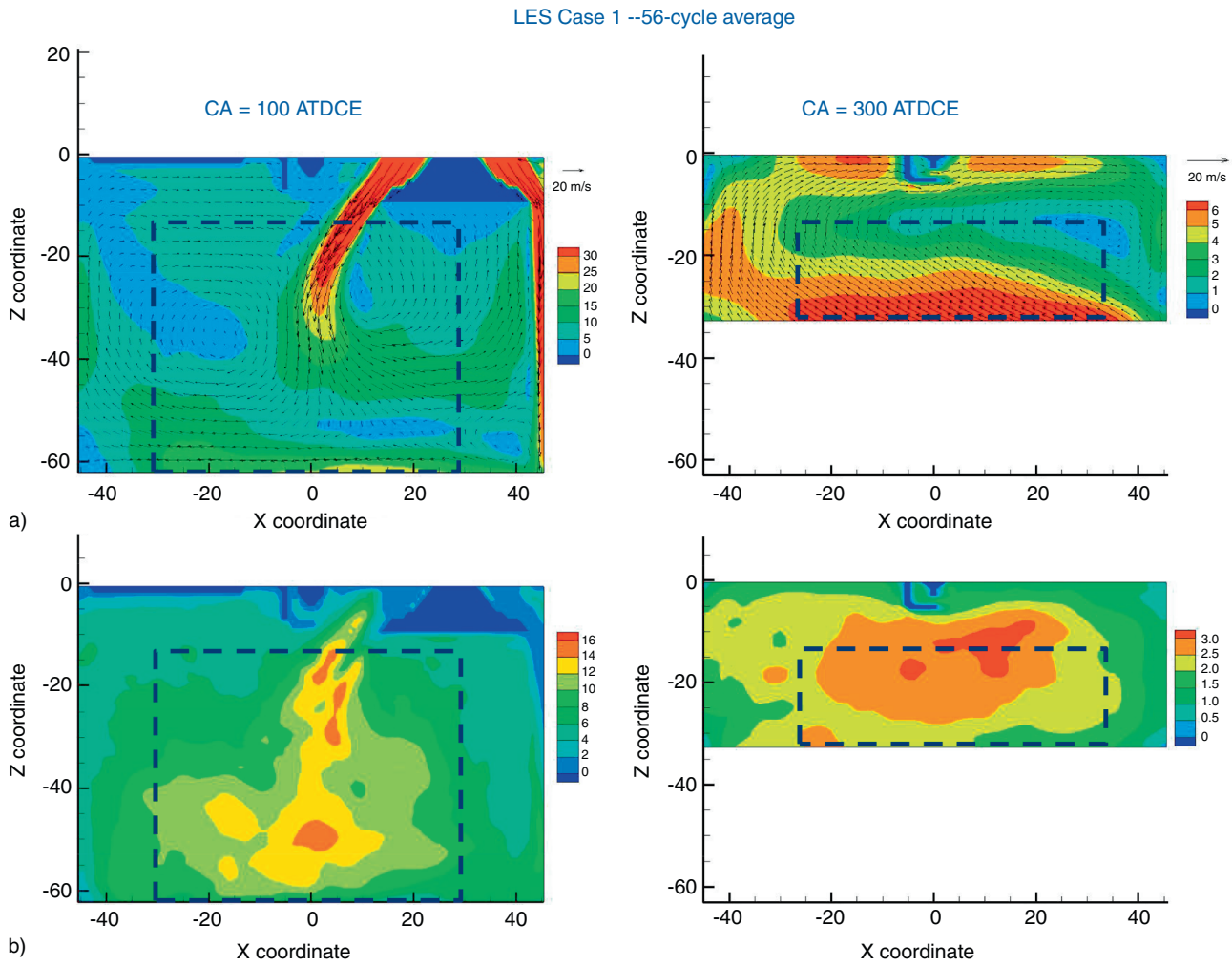

Figure 9

56-cycle average LES Case 1 results on a) mean and b) RMS velocities at 100 and 300 degree ATDCE – Case 1.

TABLE 5

Comparison of relevance index between 56-cycle average LES and PIV data over the POD analysis window

	Relevance index on mean velocity	Relevance index on RMS velocity
100 degree ATDC	0.921	0.974
300 degree ATDC	0.970	0.983

number of cycles as more energy gets redistributed into higher modes. At 100 degree ATDCE the energy fraction decreases from 0.692 to 0.645 when changing the sample from 10-cycles to 56-cycles for the PIV data. Similarly for the LES baseline (Case 1) calculations, it decreases from 0.607 to 0.569 when going from 10-cycles to 56-cycles. The absolute value of the first mode energy fraction from LES is 14% lower than the PIV measurements. However, the relative decrease in the fraction when going from 10-cycles to 56-cycles is 6.7% which is very close to the value from PIV measurements of 7.3%. This indicates that the LES computations are capturing the cycle-to-cycle variation of energy distribution among different modes.

Figure 12 shows that overall agreement in POD mode energy fraction is less at 100 degree ATDCE than 300 degree ATDC. At both crank angles, the majority of the flow energy is in the first 3 modes. However, up to 56 cycles with the corresponding 56

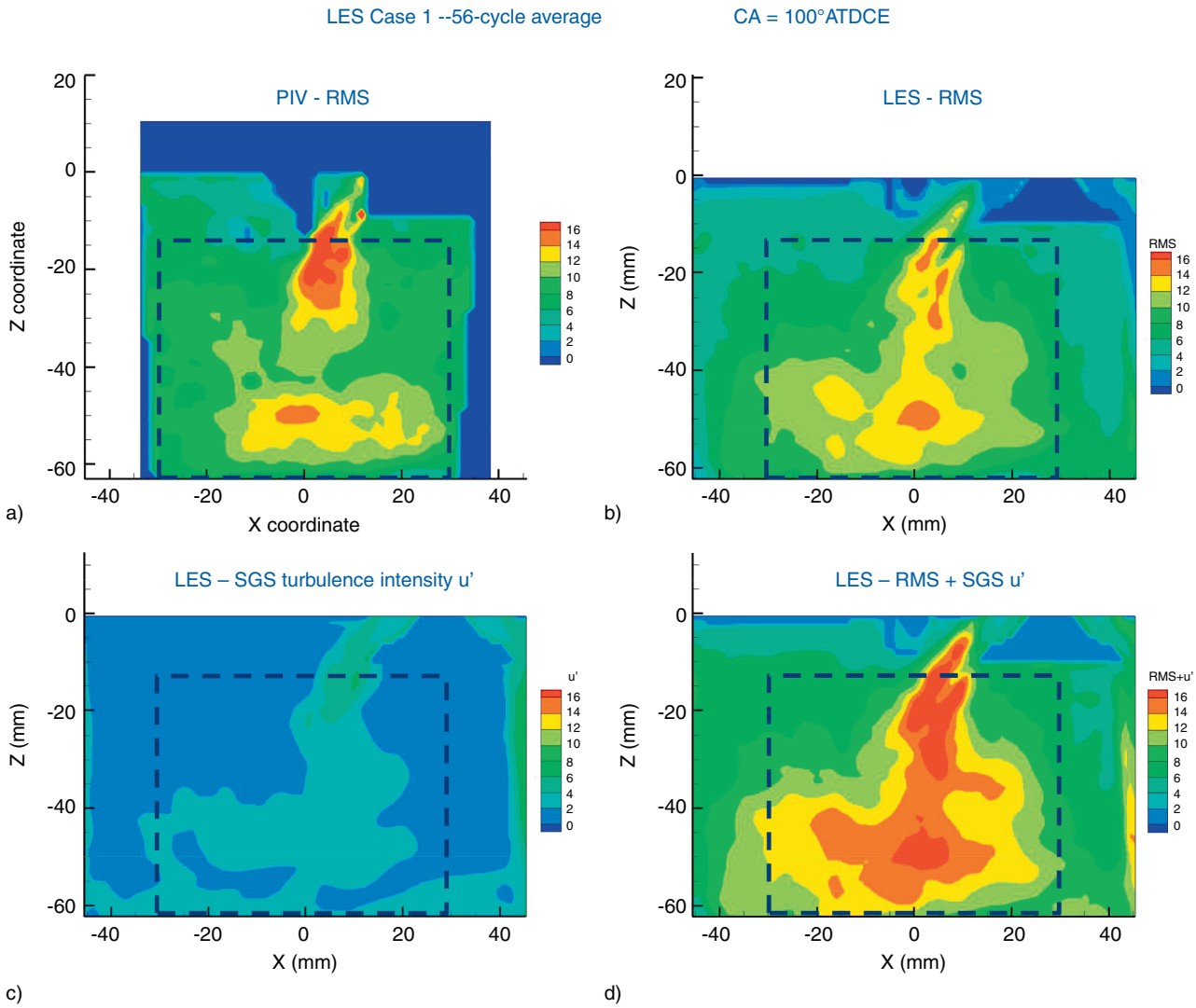

Figure 10

Comparison of a) PIV-<RMS>, b) LES-<RMS>, c) LES-SGS tubulence intensity u' and d) LES-<RMS>+SGS<u'> at 100 degree ATDCE.

modes may be required to achieve converged spectra. In most cases, the LES predicted POD energy fractions agree well with the PIV measurements at 2D cutting planes.

5.3 Number of Cycles for Convergence

Figure 13 shows the effect of cycle number on relevance index. The relevance index was computed over the whole 2-D domain between the 56-cycle average flow field and various selected number of cycle averaged flow field. By definition, as the number of cycles approaches the total number (56), the relevance index approaches 1.0. Within the first 10 cycles the relevance index for mean and RMS of computed velocity reaches values $\geq$0.98. However, 20-cycles seem to yield a slightly better relevance index $>$0.99.

In order to test the effect of sampling on the number of cycles required for convergence, the relevance index is calculated using 10-cycles at a time over the whole 2-D domain from 2nd-10 cycles to 5th-10 cycles at 100 degree and 300 degree ATDCE respectively. The results are shown in Figures 14-17. It can be seen that the change in relevance index is less than 0.5% for both

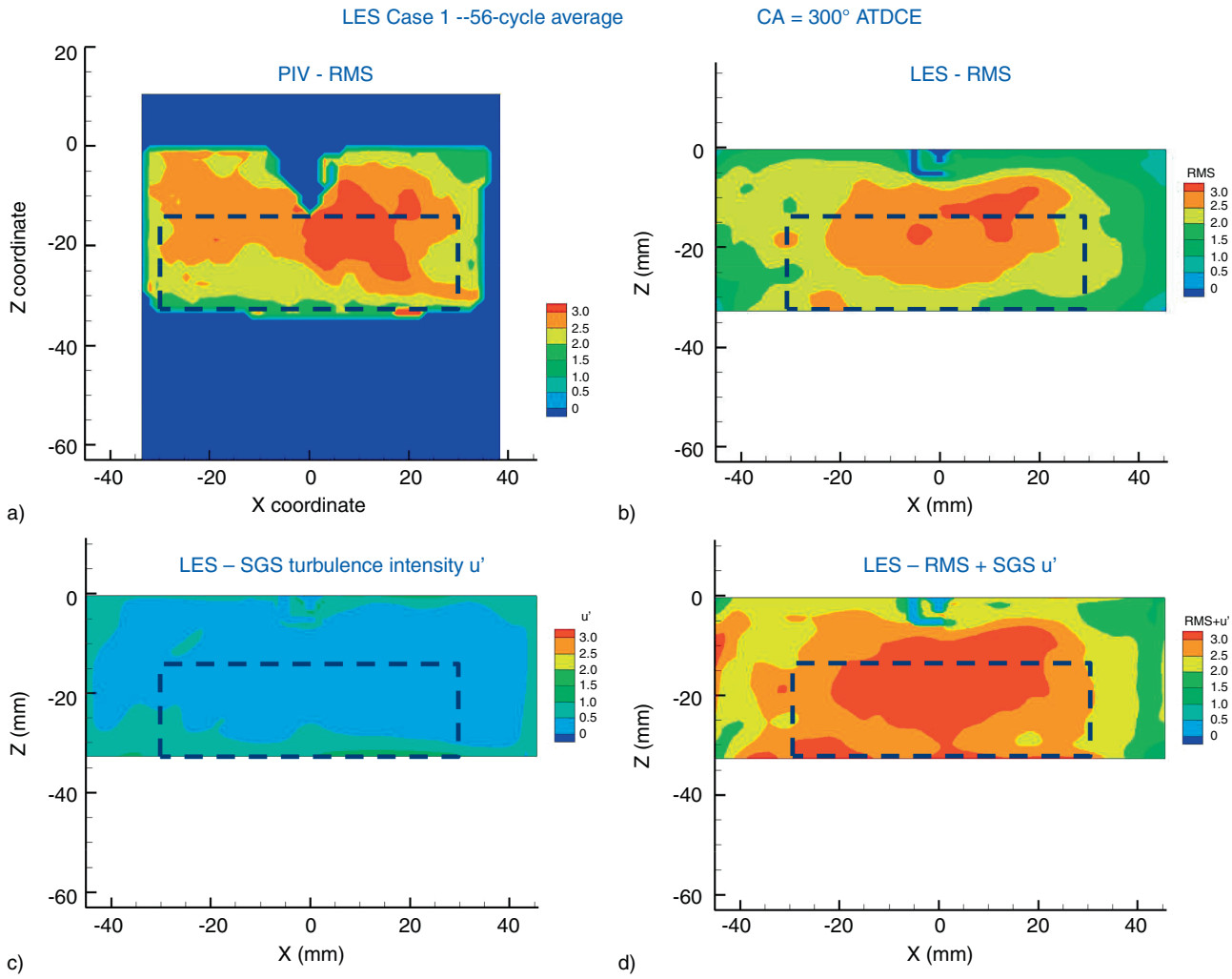

Figure 11

Comparison of a) PIV-<RMS>, b) LES-<RMS>, c) LES-SGS tubulence intensity u' and d) LES-<RMS>+SGS<u'> at 300 degree ATDCE.

mean and RMS velocity at 100 degree and 300 degree ATDCE.

Figure 18 shows the POD modes between LES and PIV measurements over the POD analysis window from 2nd-10 to 5th-10 cycles. The average energy fraction of mode 1 is 0.668 for PIV and 0.617 for LES at 100 degree ATDCE. The scatter band of the modes from 2nd-10 to 5th-10 cycles is comparable between LES and PIV measurements. This suggests 10 cycles are also sufficient for making qualitative comparison of LES and PIV measurements of mean and RMS velocity. Analysis of results at 300 degree ATDCE leads to similar conclusions.

While experimental results are available in a matter of minutes for multiple cycles after running the engine, it takes several days to get LES results of multiple cycles. Based on the above comparison, the authors choose 10 cycles in the following sensitivity studies for qualitative analysis, in order to save computing time.

5.4 Field-of-View Window Shift

Several perturbations of the field-of-view windows for POD analysis are explored on the LES results. The effect of in-plane shift of the field-of-view windows by 1-2 mm horizontally and vertically are tested. Out of plane shift

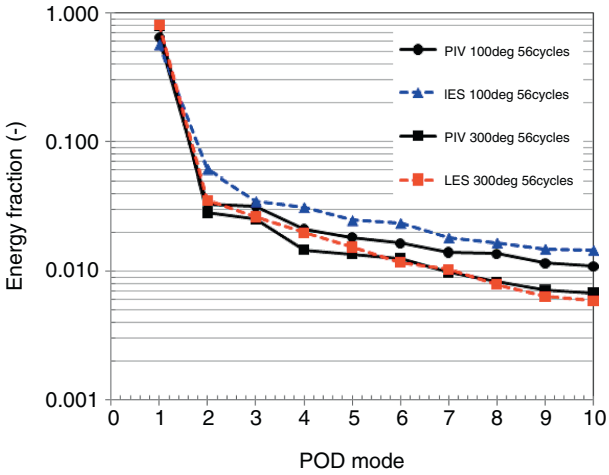

Figure 12

Fraction of kinetic energy *versus* POD mode number from 2D phase-dependent POD analysis for 56 snapshots of PIV and LES Case 1 data at 100 and 300 degree ATDCE, respectively.

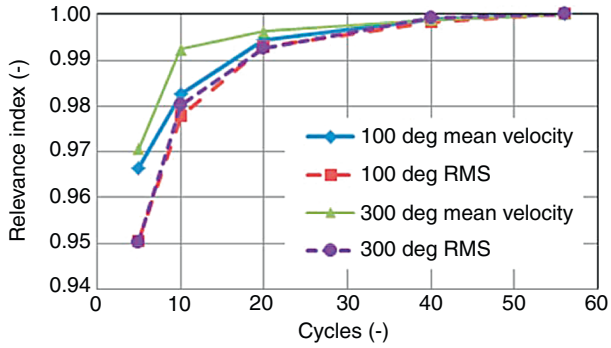

Figure 13

Effect of cycle number on relevance index.

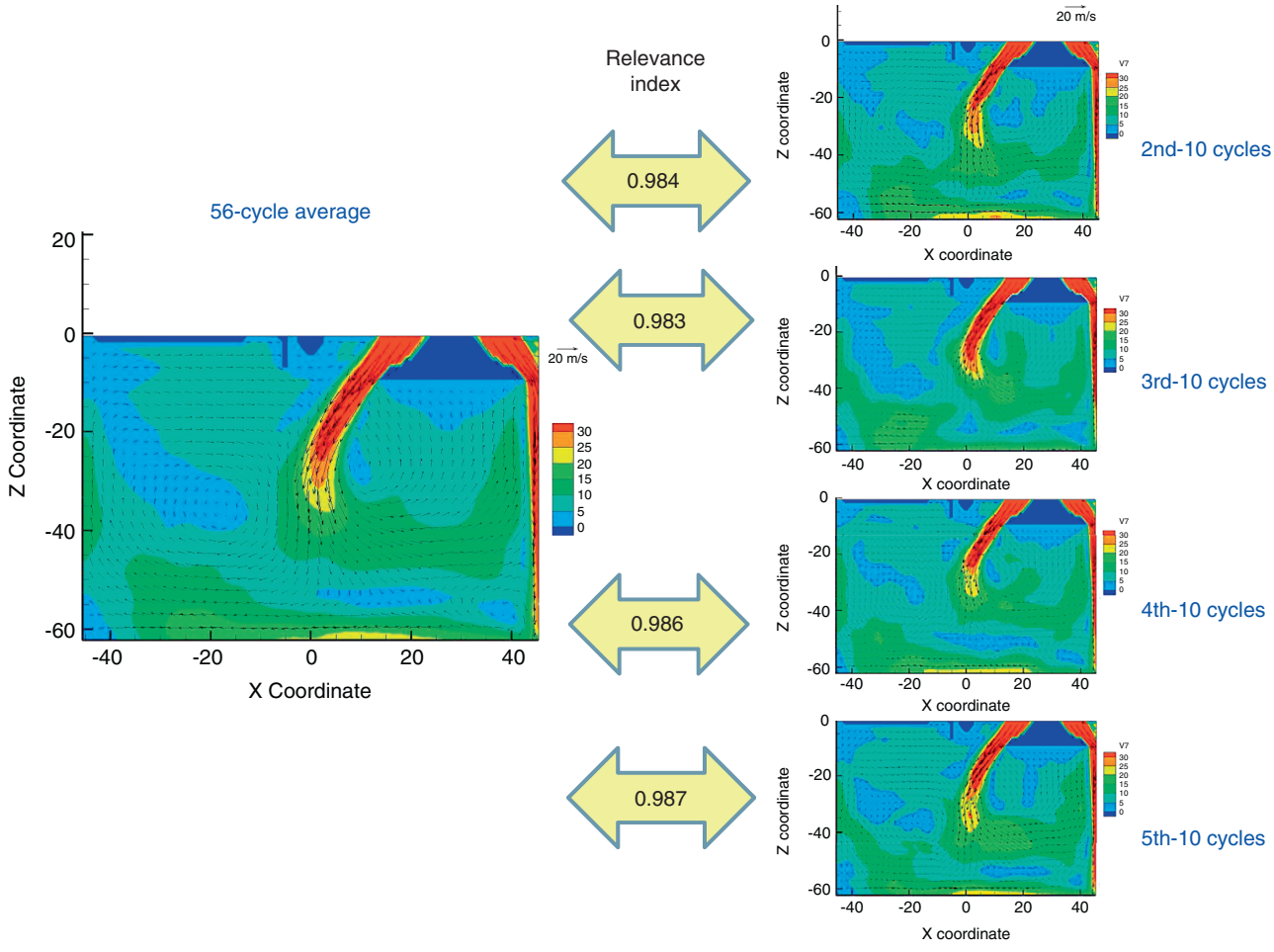

Figure 14

Comparison of mean velocities at 100 degree ATDCE.

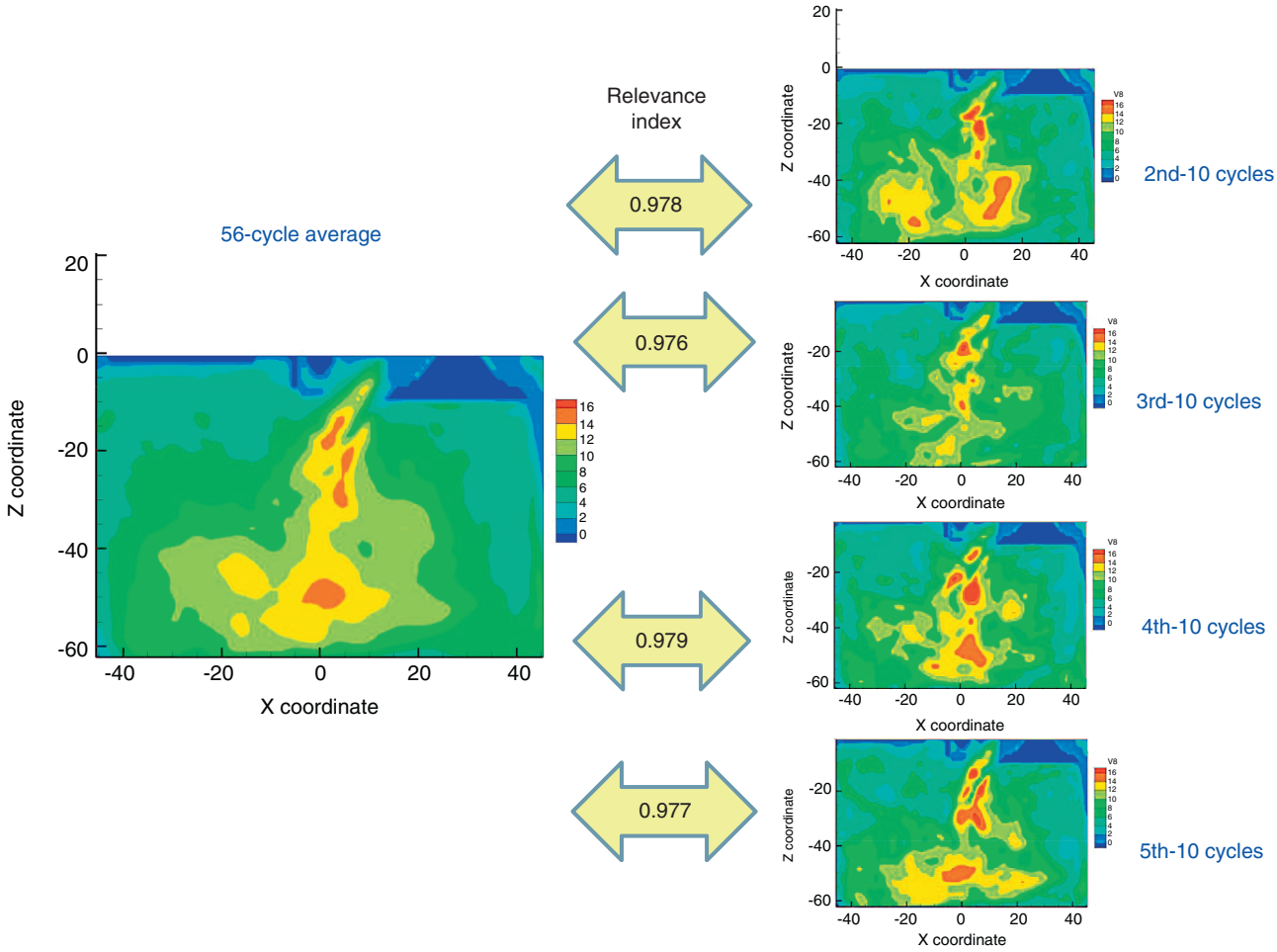

Figure 15
Comparison of RMS velocities at 100 degree ATDCE.

of 1-2 mm is also tested. The results at 100 degree ATDCE are summarized in Figure 19. At 100 degree ATDCE, the difference in energy fraction of mode 1 resulting from view window offset in *X*- and *Z*-direction is about 0.5% for 1 mm and 2% for 2 mm offset, respectively. The difference in energy fraction of mode 1 resulting from view windows offset in *Y*-direction (perpendicular to the view area) is about 2% for 1 mm and 3% for 2 mm offset at 100 degree ATDCE. This is larger than the values observed in the other two directions (*X* and *Z*). Similar results are observed at 300 degree ATDCE view window offset.

In summary, for all cases examined, the variation in energy fraction of mode 1 was judged to be very small on the order of 1-3% compared to the original view window. These findings are encouraging since they indicate low sensitivity to small changes in the measurement location.

6 SENSITIVITY ANALYSIS

6.1 In-Cylinder Mesh Size (Cases 1, 2 and 3)

The effect of mesh size on the predicted LES results is presented in this section. Figure 20 shows the POD energy modes from LES computations with 0.75 (Case 2), 1.00 (Case 1) and 2.00 (Case 3) mm mesh along with the POD modes from PIV measurements at 100 and 300 degrees ATDCE. The overall agreement is better with a 1.00 mm mesh. This is probably because of the model constants that were chosen (*Tab. 3*) were

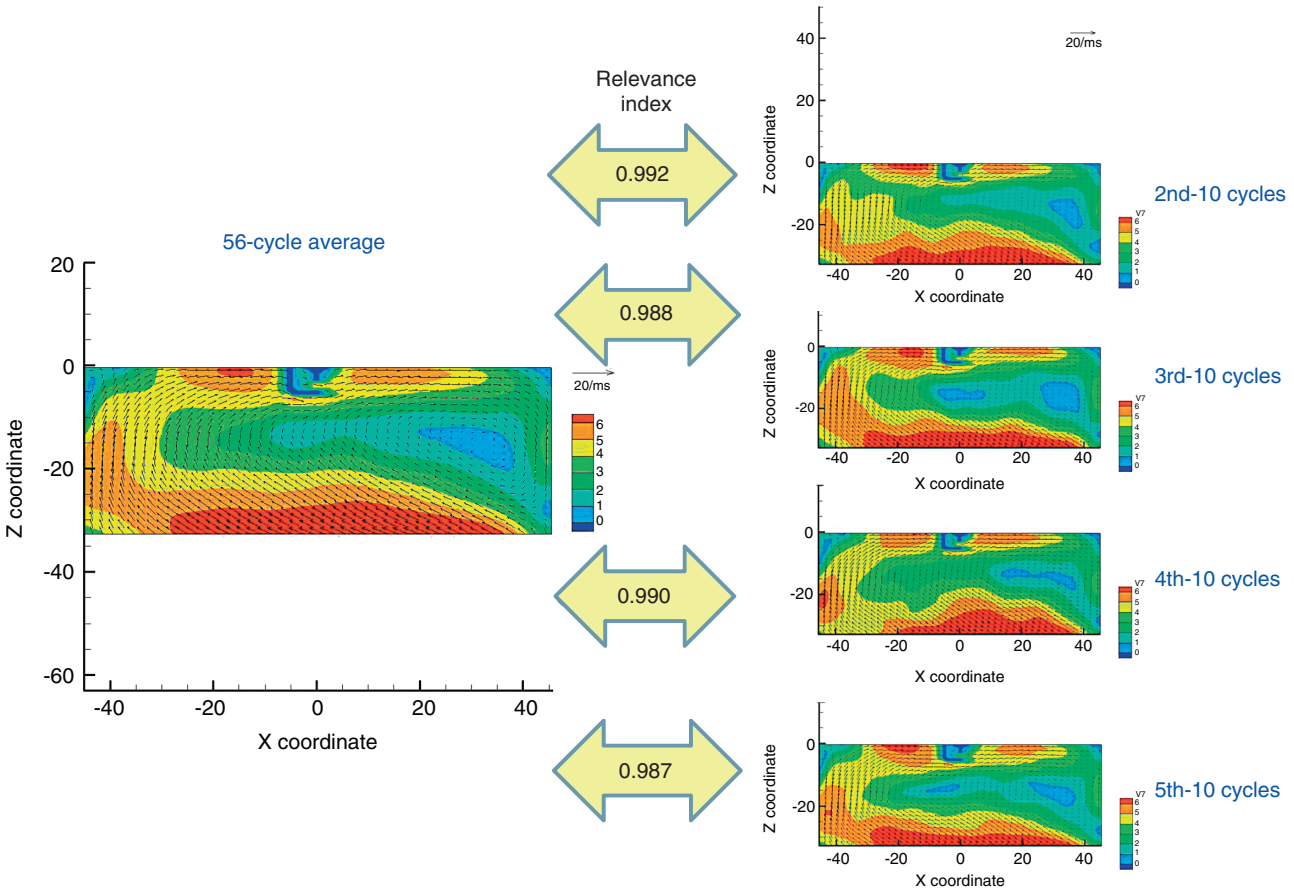

Figure 16

Comparison of mean velocities at 300 degree ATDCE.

optimized for mesh sizes close to 1.00 mm. For the readers reference, a mesh size of 0.75 to 1.00 mm is less than the turbulent length scale ($L_T \sim 0.25 \times$ TDC clearance height) of 3 mm and larger than the Kolmogorov length scale of 0.0343 mm ($\eta = L_T \mathrm{Re}^{-3/4}$). The size of near-wall cell varies from 0.5 to 1 mm.

6.2 Time Step (Cases 1 and 4)

The use of a minimum fixed time step in the computation (Case 4) is tested against the use of adaptive time step as determined by the CFD code (Case 1). The mean and RMS distributions do not show significant difference as well as the POD energy modes shown in Figure 21 (First mode energy fraction differs by 1.5% and 8% at 100 and 300 degree ATDCE, respectively). However, the minimum fixed time step case took 3-4 times longer to run than that of the adaptive time step. Hence, adaptive time step is recommended for non-reacting flow LES.

6.3 Viscosity Models (Cases 1 and 5)

The numerical treatment of turbulent viscosity using zero-equation Smagorinsky model (Case 5) is tested against the one equation SGS (Case 1) model. The mean and RMS distributions do not show significant difference as well as the POD energy modes shown in Figure 22 (first mode energy fraction differs by 1.5% and 8% at 100 and 300 degree ATDCE, respectively). Hence, the SGS turbulent model does not seem to matter for non-reacting flow. For reacting flows, however, this might not be the case. This needs to be verified as part of future work.

6.4 Boundary Conditions Specification – With and Without GT-Power Calculated Values (Cases 1, 6-8)

A detailed study of the various types of boundary conditions for the simulations was performed. Static and dynamic pressure boundary conditions and steady and time-varying pressure boundary conditions were used for multi-cycle

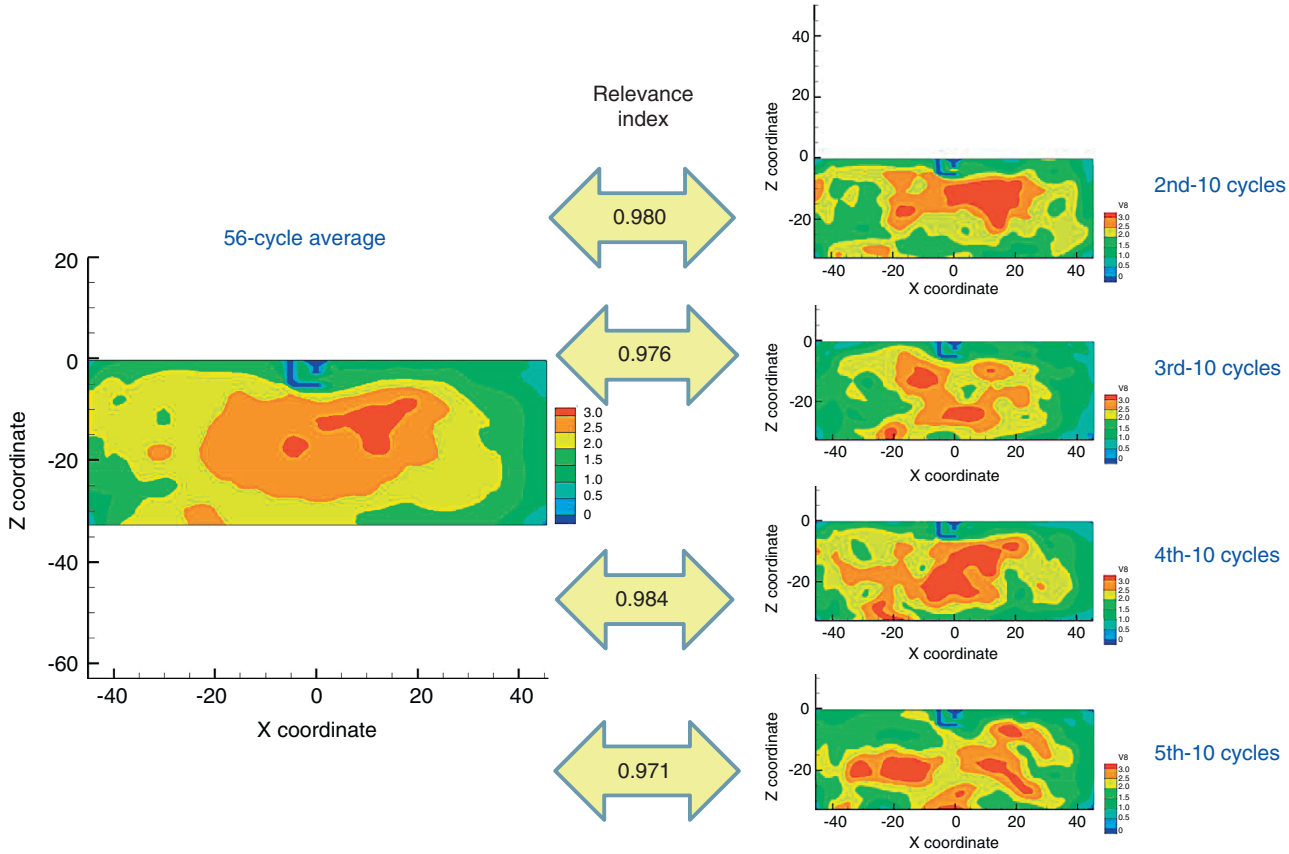

Figure 17

Comparison of RMS velocities at 300 degree ATDCE.

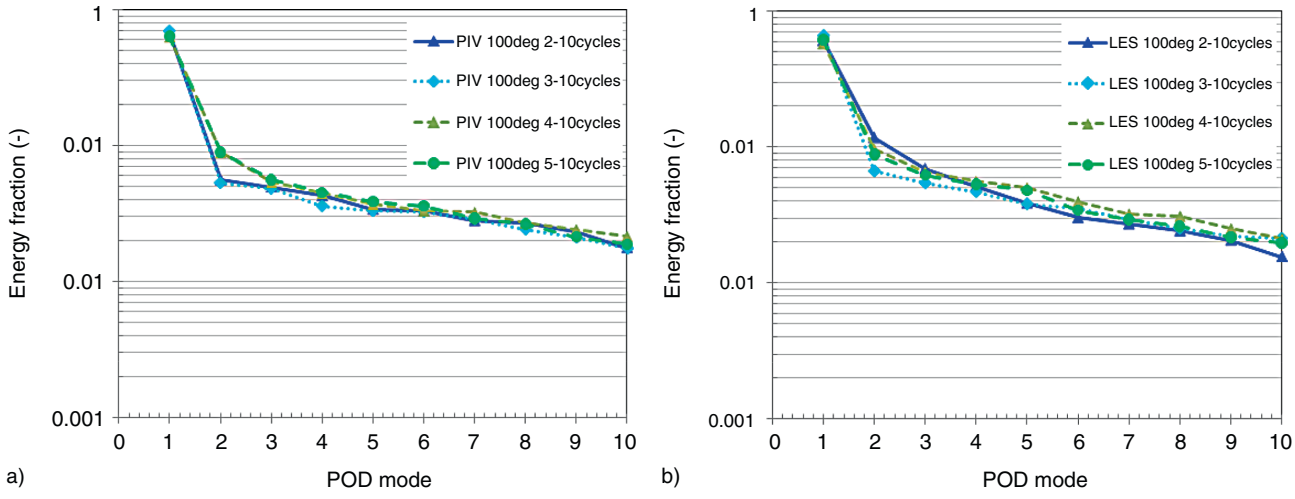

Figure 18

Comparison of fraction of kinetic energy *versus* POD mode number from 2D phase-dependent POD analysis between PIV and LES for individual 10 snapshots for Case 1 at 100 degree ATDCE.

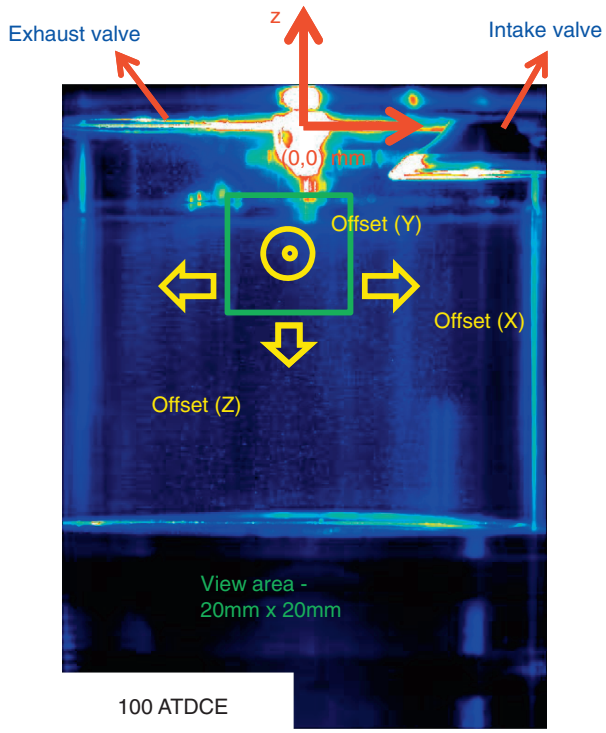

	Energy fraction mode 1%	Difference %
Original	0.7856	0
X -1 mm	0.7897	0.5147
X -2 mm	0.7948	1.1632
X +1 mm	0.7821	-0.4504
X +2 mm	0.7798	-0.7412
Z -1 mm	0.7797	-0.7500
Z -2 mm	0.7720	-1.7283

	Energy fraction mode 1%	Difference %
Original	0.7856	0
Y -1 mm	0.7705	-1.9224
Y -2 mm	0.7649	-2.6353
Y +1 mm	0.7926	0.8911
Y +2 mm	0.7847	-0.1121

Figure 19

Effect of view window offset on energy fraction of mode 1 for Case 1 at 100 degree ATDCE.

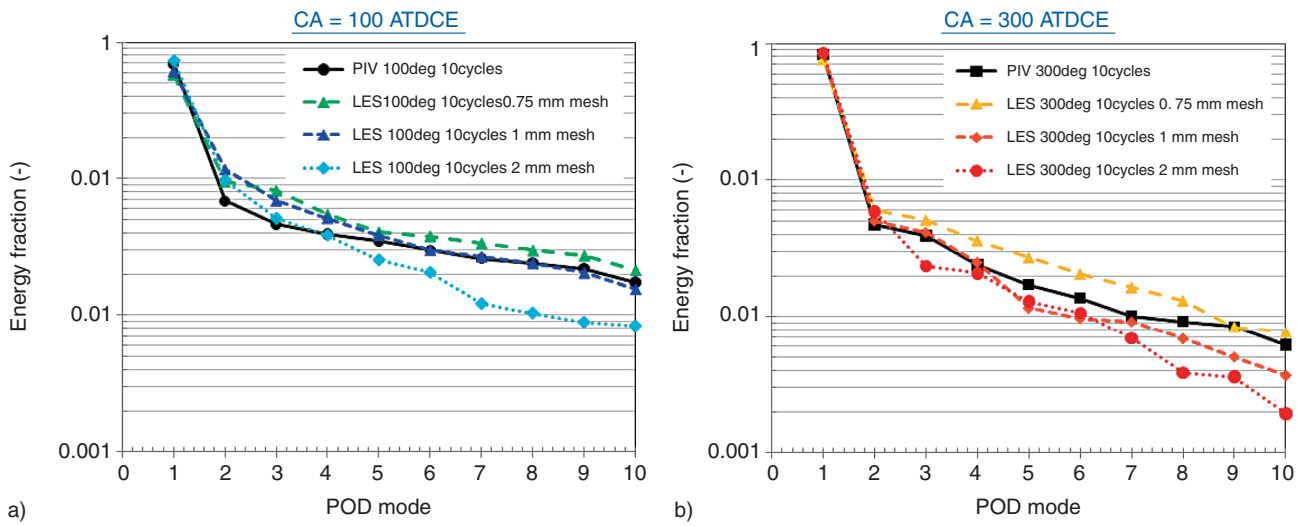

Figure 20

Fraction of kinetic energy *versus* POD mode number from 2D phase-dependent POD analysis for 10 snapshots of PIV and LES Cases 1, 2 and 3 data at a) 100 and b) 300 degree ATDCE, respectively.

LES studies (often 20+ cycles). The unsteady boundary conditions were available from both measured data and 1-D system simulations. The primary evaluation criteria were peak cylinder average pressure and trapped cylinder mass. Comparison between simulations and experiments shows that time varying pressure boundary conditions

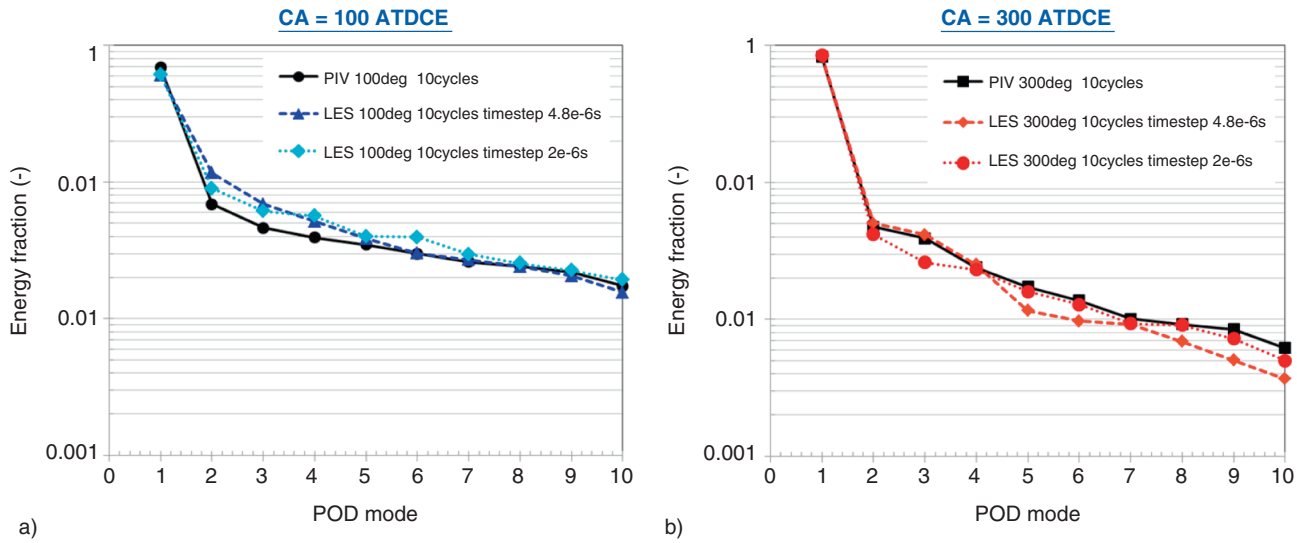

Figure 21

Fraction of kinetic energy *versus* POD mode number from 2D phase-dependent POD analysis for 10 snapshots of PIV and LES Cases 1 and 4 data at 100 and 300 degree ATDCE, respectively.

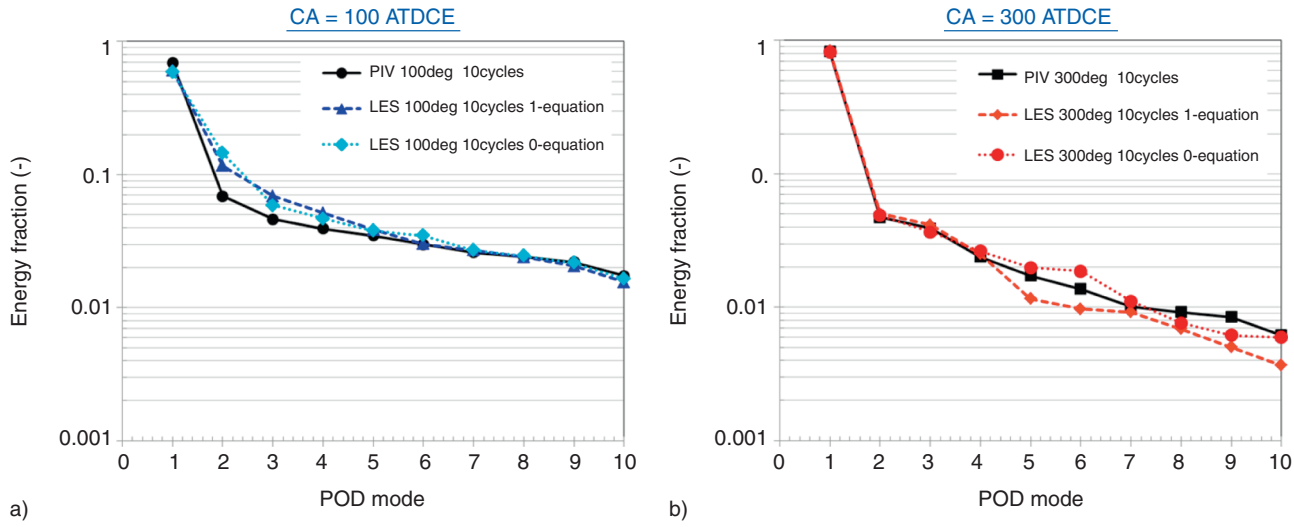

Figure 22

Fraction of kinetic energy *versus* POD mode number from 2D phase-dependent POD analysis for 10 snapshots of PIV and LES Cases 1 and 5 data at 100 and 300 degree ATDCE, respectively.

provided more accurate simulation results and the LES simulations were able to capture cyclic variations.

The following recommendations can be made as a result of this study:

– both measured and GT-Power calculated pressures are acceptable for use as inlet boundary condition;
– mesh size sensitive study indicates that it is acceptable for mesh size of 1 mm or less, while 2 mm is too coarse;
– inlet of intake plenum is good location for boundary condition specification. The predicted POD energy fractions are similar between time varying and fixed total pressure boundary conditions;

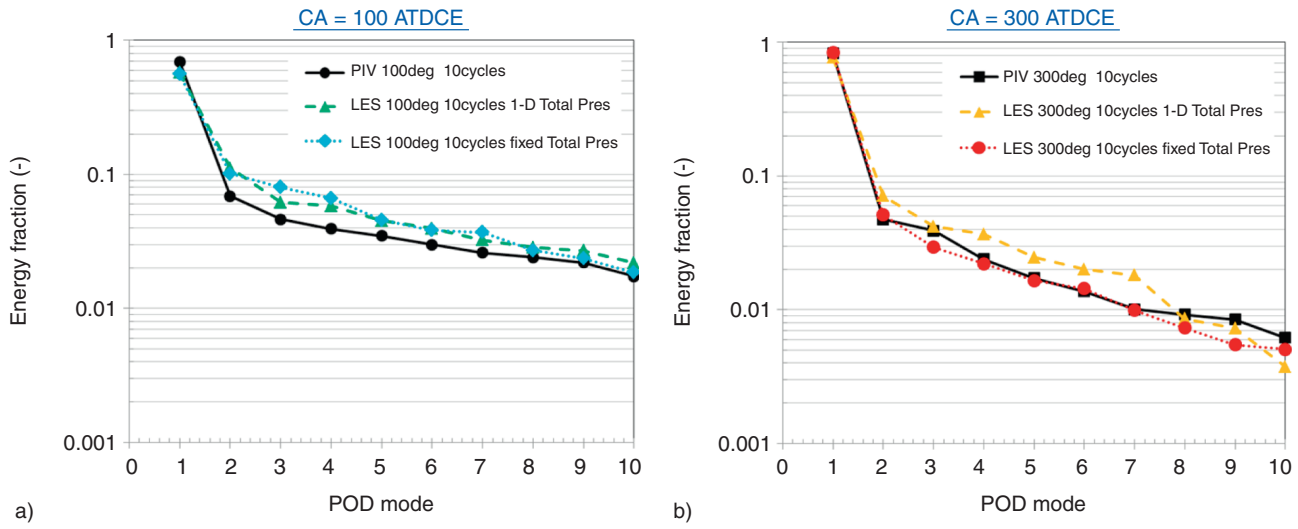

Figure 23

Fraction of kinetic energy *versus* POD mode number from 2D phase-dependent POD analysis for 10 snapshots of PIV and LES Cases 1, and 6 data at 100 and 300 degree ATDCE, respectively.

– similar results were also obtained between cases with:
  – time-varying and fixed (> 4.8e-06 and 2e-6 second, respectively) time steps,
  – zero- and 1-Eqn eddy viscosity models,
  – time-varying and fixed total pressure BC (*Fig. 23*).

SUMMARY AND CONCLUSIONS

A concerted experimental and numerical effort is undertaken to understand and describe the nature of stochastic flows in internal combustion engines. A working group was formed to develop the tools and processes for using Large Eddy Simulation (LES) effectively and accurately to simulate IC engines.

Simulation is carried out using an engineering-level LES model that is provided by a commercial CFD code CONVERGE. A rigorous working procedure for comparing and analyzing the results from simulation and experiments is documented in this paper. This procedure is then employed to explore the following aspects:

– effect of numerical parameters (mesh size and time step), Sub-Grid-Scale (SGS) turbulence models and boundary condition treatments on LES predictions;
– number of cycles required for convergence with adequate accuracy;
– application of the Proper Orthogonal Decomposition (POD) analysis technique.

The analysis procedure and simulation capability developed in this paper will be applied to explore linkage between flow field and flame interactions with homogeneous-charge combustion currently under investigation.

Major findings of the present study include:

– a GT-Power model was developed to accurately replicate inlet and outlet boundary conditions for LES simulation. The 1-D model predictions showed good agreement with cycle-resolved pressure measurements at selected monitoring locations in the cylinder, plenums, ports and runners;
– 1 mm mesh size in cylinder and ports is recommended for LES calculation. The default LES model constants seem to work well with this mesh size;
– inlet of intake plenum is good location for boundary condition specification. The predicted POD energy fractions are similar between time varying and fixed total pressure boundary conditions;
– calculated in-cylinder trapped mass reached quasi-steady value after 3 engine cycles. Cycle-to-cycle variations of in-cylinder pressure and trapped mass were captured well with LES calculations;
– LES-predicted mean and RMS velocities agree very well with the PIV measurements at 100 and 300 degree ATDCE, respectively;
– LES-predicted POD energy fractions also agree well with the PIV measurements at selected 2-D cutting planes and crank angle positions (2D phase-dependent POD);

– difference in POD energy fraction of mode 1 resulted from view window offset is less than 3% for 2 mm offset at 100 degree CA and less than 1% for 2 mm offset at 300 degree CA;
– quantitative comparison between LES and PIV data was carried out with 56 cycles. Our analysis suggests that 10 cycles is sufficient for qualitative analysis.

ACKNOWLEDGMENTS

The authors thank Professor Volker Sick, Professor Dan Haworth, Professor Chris Rutland and Drs. Dave Reuss and Saurabh Gupta for many helpful and enlightening discussions, and Dr. Eric Pomraning, Dr. Yunliang Wang and Dr. Keith Richards at CSI for their support of LES simulation.

REFERENCES

1 Sick V., Reuss D., Rutland C., Haworth D., Oefelein J., Janicka J., Kuo T.-W., Yang X., Freitag M. (2010) A Common Engine Platform for Engine LES Development and Validation, *LES4ICE Conference*, Rueil-Malmaison, France, 18-19 Nov.

2 *CONVERGE^{TM}: A Three-Dimensional Computational Fluid Dynamics Program for Transient Flows with Complex Geometries*, Convergent Science Inc. (2009).

3 Smagorinsky J. (1963) General circulation experiments with the primitive equations, *Month. Weath. Rev.* **91**, 99-164.

4 Lilly D.K. (1992) A proposed modification of the Germano sub-grid-scale closure method, *Phys. Fluids A* **4**, 633-635.

5 Yoshizawa A., Horiuti K. (1985) A statistically-Derived Subgrid-Scale Kinetic Energy Model for the Large-Eddy Simulation of Turbulent Flows, *J. Phys. Soc. Jpn* **54**, 8, 2834-2839.

6 Menon S., Yeung P.K., Kim W.W. (1996) Effect of Subgrid Models on the Computed Interscale Energy Transfer in Isotropic Turbulence, *Comput. Fluids* **25**, 2, 165-180.

7 Ghosal S., Lund T.S., Moin P., Akselvoll K. (1995) A dynamic localization model for large-eddy simulation of turbulent flows, *J. Fluid Mech.* **286**, 229-255.

8 Pomraning E., Rutland C.J. (2002) A Dynamic One-Equation Non-Viscosity LES Model, *AIAA J.* **40**, 4, 689-701.

9 Werner H., Wengle H. (1993) Large-Eddy Simulation of Turbulent Flow Over and Around a Cube in a Plate Channel, *Turbulent Shear Flows* **8**, 155-168.

10 Liu K., Haworth D. (2011) Development and Assessment of POD for Analysis of Turbulent Flow in Piston Engines, *SAE paper* 2011-01-0830.

11 Berkooz G., Holmes P., Lumley J.L. (1993) The proper Orthogonal Decomposition in the Analysis of Turbulent Flows, *Annu. Rev. Fluid Mech.* **25**, 16, 539-575.

12 Sirovich L. (1987) Turbulence and the Dynamics of Coherent Structures, *Quarterly Appl. Math.* **45**, 561-590.

13 Manhart M., Wengle H. (1993) A Spatiotemporal Decomposition of a Fully Inhomogeneous Turbulent Flow Field, *Theor. Comput. Fluid Dyn.* **5**, 6, 233-242.

14 Abraham P., Liu K., Haworth D., Reuss D., Sick V. (2012) Evaluating LES AND High-speed PIV with Phase-invariant POD, LES4ICE Conference, Rueil-Malmaison, France, 29-30 Nov.

15 Rutland C., Van Dam N., Sick V., Reuss D., Haworth D., Oefelein J., Kuo T.-W., Yang X. (2012) A Common Engine Platform for Engine LES Development and Validation, LES4ICE Conference, Rueil-Malmaison, France, 29-30 Nov.

Manuscript accepted in February 2013
Published online in October 2013